


 Cite this: *RSC Adv.*, 2021, 11, 9395

# Fe<sub>2</sub>O<sub>3</sub> enhanced high-temperature arsenic resistance of CeO<sub>2</sub>–La<sub>2</sub>O<sub>3</sub>/TiO<sub>2</sub> catalyst for selective catalytic reduction of NO<sub>x</sub> with NH<sub>3</sub>

 Na Wang,<sup>a</sup> Changfei Ye,<sup>a</sup> Huidong Xie,<sup>\*b</sup> Chang Yang,<sup>c</sup> Jinhong Zhou<sup>d</sup> and Chengmin Ge<sup>e</sup>

High-temperature arsenic resistance catalysts of CeLa<sub>0.5</sub>Fe<sub>x</sub>/Ti ( $x = 0, 0.1, 0.2, 0.3, 0.4, 0.5$ ) series were prepared and measured under a simulation condition of arsenic poisoning. The as-prepared catalysts were characterized by XRD, SEM, TEM, and XPS. The specific surface area and pore size of the catalysts were measured. At  $x = 0.2$ , the catalyst shows the best arsenic resistance and catalytic performance. The active temperature range of the CeLa<sub>0.5</sub>Fe<sub>0.2</sub>/Ti catalyst is 345–520 °C when the gas hourly space velocity is up to 225 000 mL g<sup>-1</sup> h<sup>-1</sup>. Compared with commercial vanadium-based catalysts, CeLa<sub>0.5</sub>Fe<sub>0.2</sub>/Ti shows much better catalytic performance. The introduction of Fe will improve the dispersion of CeO<sub>2</sub> and increase the concentration of Ce<sup>3+</sup> and unsaturated active oxygen on the surface. The NH<sub>3</sub>-TPD and H<sub>2</sub>-TPR results show that the CeLa<sub>0.5</sub>Fe<sub>0.2</sub>/Ti catalyst has more acidic sites and more excellent redox performance than CeLa<sub>0.5</sub>Fe<sub>0</sub>/Ti. The CeLa<sub>0.5</sub>Fe<sub>0.2</sub>/Ti catalyst might have application prospects in the field of selective catalytic reduction of NO<sub>x</sub> with NH<sub>3</sub>.

 Received 3rd January 2021  
 Accepted 8th February 2021

DOI: 10.1039/d1ra00031d

[rsc.li/rsc-advances](http://rsc.li/rsc-advances)

## 1. Introduction

Nitrogen oxides (NO<sub>x</sub>) are some of the main pollutants in the atmosphere, which can do great harm to the ecological environment and human health, such as, acid rain, photochemical smog, ozone depletion, *etc.*<sup>1</sup> Selective catalytic reduction (SCR) of NO<sub>x</sub> with ammonia is the most effective method to reduce NO<sub>x</sub> in flue gas of stationary sources. Currently, the most widely used commercial SCR catalyst is V<sub>2</sub>O<sub>5</sub>–WO<sub>3</sub>(MoO<sub>3</sub>)/TiO<sub>2</sub>.<sup>2,3</sup> The vanadium-based catalyst has many advantages as well as some unavoidable problems, such as, strong biological toxicity of vanadium, narrow temperature window (300–400 °C), easy oxidation of SO<sub>2</sub> to SO<sub>3</sub>, and low N<sub>2</sub> selectivity at high temperature.<sup>4</sup> Recent reports have shown that CeO<sub>2</sub> is the most powerful substitute for V<sub>2</sub>O<sub>5</sub> because of its non-toxicity, high reactivity, and excellent oxygen storage and release capabilities.<sup>5–7</sup> However, the adaptability and anti-inactivation ability of

CeO<sub>2</sub> in a complicated flue gas environment is still an urgent problem to be solved. Heavy metal arsenic, often existing in the form of volatile As<sub>2</sub>O<sub>3</sub> or As<sub>2</sub>O<sub>5</sub> in high-temperature flue gas, is toxic to commercial SCR catalysts.<sup>8</sup> Early reports show that the arsenic poisoning of commercial catalysts is due to the coverage of the active sites on the surface of the catalyst by inactive As<sub>2</sub>O<sub>5</sub> and the diffusion of arsenic oxides into the pores of the catalyst, which causes the blocking of the micropores in the catalysts.<sup>9–11</sup> The current widely accepted view is that chemical deactivation is the main reason, because arsenic of high oxidation state, As(v), can interact with the active site of vanadium to reduce the surface acid sites.<sup>12–14</sup> In order to improve the arsenic resistance, commercial vanadium-based catalysts often need many additives, such as WO<sub>3</sub> and MoO<sub>3</sub>. It has been found that MoO<sub>3</sub> has better resistance to arsenic poisoning than WO<sub>3</sub> because MoO<sub>3</sub> can further improve the dispersion of active sites of vanadium.<sup>15</sup> Current literature on arsenic resistance mainly focuses on adding MoO<sub>3</sub> to commercial vanadium-based catalysts. However the highest NO conversion of these catalysts after arsenic poisoning is less than 80%.<sup>16,17</sup> It is also effective in improving the arsenic resistance of CeO<sub>2</sub>-based catalysts by adding WO<sub>3</sub>/MoO<sub>3</sub>.<sup>18–20</sup> However the reported highest NO conversion of the CeO<sub>2</sub>-based catalysts after arsenic poisoning is only 75%. So far, there is no report on the CeO<sub>2</sub>-based catalyst by adding Fe<sub>2</sub>O<sub>3</sub> as arsenic resistance catalyst. Recently, our research group has developed the CeO<sub>2</sub>–La<sub>2</sub>O<sub>3</sub>/TiO<sub>2</sub> vanadium-free catalysts, which can be used at high temperature and are expected to replace commercial vanadium-based catalysts. Owing to its catalytic activity, sulfur resistance and porous properties, TiO<sub>2</sub> is an excellent catalytic carrier. La<sub>2</sub>O<sub>3</sub> is a good auxiliary component for

<sup>a</sup>College of Architecture and Civil Engineering, Xi'an University of Science and Technology, Xi'an, 710054, Shaanxi, China. E-mail: wangna811221@xust.edu.cn; Fax: +86-29-82202335; Tel: +86-29-82203378

<sup>b</sup>School of Chemistry and Chemical Engineering, Division of Laboratory and Equipment Management, Xi'an University of Architecture and Technology, Xi'an, 710055, Shaanxi, China. E-mail: xiehuidong@tsinghua.org.cn

<sup>c</sup>Division of Laboratory and Equipment Management, Xi'an University of Architecture and Technology, Xi'an, 710055, Shaanxi, China

<sup>d</sup>College of Geography and Environment, Baoji University of Arts and Sciences, Baoji, 721013, Shaanxi, China

<sup>e</sup>Shandong Dongyuan New Material Technology Co., Ltd, Dongying, 257300, Shandong, China



active component of CeO<sub>2</sub> because of the formation of Ce–O–La bond on the surface of CeO<sub>2</sub>, which increases the acidic sites of the catalyst and the adsorption of NH<sub>3</sub> and NO. Because Fe-based catalysts have good deNO<sub>x</sub> performance<sup>21,22</sup> as well as good adsorption of arsenic owing to the formation of strong Fe–O–As chemical bond in the removal of the arsenic in the water treatment,<sup>23–26</sup> it is expected that Fe<sub>2</sub>O<sub>3</sub> can be used as an arsenic resistance catalyst. In this paper, the Ce–La–Fe–Ti catalysts were obtained by an impregnation method, using anatase as the carrier and Ce–La–Fe oxides as the active component. The deNO<sub>x</sub> activity of the as-prepared catalysts was measured. The as-prepared catalysts were characterized by XRD, SEM, TEM, and XPS. The reason for the arsenic resistance was discussed.

## 2. Experimental

### 2.1 Reagents and preparation

The Ce–La–Fe–Ti composite catalysts were prepared by an impregnation method. First, a certain volume of deionized

$$\text{N}_2 \text{ selectivity (\%)} = \frac{[\text{NO}]_{\text{in}} - [\text{NH}_3]_{\text{in}} - [\text{NO}_2]_{\text{out}} - 2[\text{N}_2\text{O}]_{\text{out}} - [\text{NO}]_{\text{out}} - [\text{NH}_3]_{\text{out}}}{[\text{NO}]_{\text{in}} + [\text{NH}_3]_{\text{in}} - [\text{NO}]_{\text{out}} - [\text{NH}_3]_{\text{out}}} \times 100\% \quad (2)$$

water was added to a stainless steel reactor and heated to 60 °C. Then ammonia (25–28 wt%) and citric acid (analytical purity) were added to adjust the pH to 3–4 with stirring. After that, anatase pigment (TiO<sub>2</sub>, industrial grade), Ce(NO<sub>3</sub>)<sub>3</sub>·6H<sub>2</sub>O (industrial grade), La(NO<sub>3</sub>)<sub>3</sub>·6H<sub>2</sub>O (industrial grade), and (NH<sub>4</sub>)<sub>2</sub>Fe(SO<sub>4</sub>)<sub>2</sub>·6H<sub>2</sub>O (analytical purity) were added according to the different weight ratios, CeLa<sub>0.5</sub>Fe<sub>x</sub>/Ti (*x* = 0, 0.1, 0.2, 0.3, 0.4, 0.5), where 0.5 and *x* are the weight ratios of La (calculated as La<sub>2</sub>O<sub>3</sub>) and Fe (calculated as Fe<sub>2</sub>O<sub>3</sub>) to Ce (calculated as CeO<sub>2</sub>). In all the Ce–La–Fe–Ti composite catalysts, the weight ratio of Ce–La–Fe to Ti (calculated as TiO<sub>2</sub>) is 3 : 7. The suspension was stirred continuously for 2–3 h and evaporated by vacuum distillation for 1 h. Then the mixture was cooled to room temperature, ripen for 2 hours, dried at 105 °C for 12 h, and calcined at 500 °C in a muffle furnace for 5 h. Finally, the samples were used for the SCR activity test. For comparison, commercial vanadium-based catalysts obtained from the market were also used.

### 2.2 Catalyst activity tests

First, 1 g as-prepared catalysts were ground in a planetary ball mill for 90 min and soaked in 25 mL 1 mg mL<sup>−1</sup> arsenic standard solution (calculated as As<sub>2</sub>O<sub>3</sub>) for 3 h to simulate its arsenic poisoning. The water solvent was completely evaporated, thus the loading amount of As<sub>2</sub>O<sub>3</sub> on the catalyst was calculated to be about 2.5 wt%. Then the catalyst was adhered to an industrial honeycomb-shaped cordierite cylinder with size of φ20 × L50. After drying at 105 °C, the loaded cylinder was calcined in a closed tube furnace at 450 °C for 3 h. Then the loaded cylinder was put into a quartz tube furnace to test

the activity of the catalyst. The loading amount of the catalyst is 0.8 g. The gas composition is 500 ppm NO, 500 ppm NH<sub>3</sub>, 300 ppm SO<sub>2</sub>, 3% O<sub>2</sub>, 5% H<sub>2</sub>O, and N<sub>2</sub> is used as the balance gas. The total gas flow is 3000 mL min<sup>−1</sup>, hence the corresponding gas hourly space velocity (GHSV) is calculated to be 225 000 mL g<sup>−1</sup> h<sup>−1</sup>. The outlet gas concentrations of NO, NO<sub>2</sub>, SO<sub>2</sub> were detected by the Germany Ecom flue gas analyzer and the N<sub>2</sub>O concentration was detected by the KRM50 infrared flue gas analyzer. The temperature program was controlled by a computer. At each temperature, the experiment was kept for 30 min to stabilize before the data collection of the concentration of the outlet gas. The NO conversion and N<sub>2</sub> selectivity were calculated according to the formula (1) and (2).<sup>27,28</sup>

$$\text{NO conversion (\%)} = \frac{[\text{NO}]_{\text{in}} - [\text{NO}]_{\text{out}}}{[\text{NO}]_{\text{in}}} \times 100\% \quad (1)$$

### 2.3 Characterization

The Brunauer–Emmet–Teller (BET) specific surface area and pore volume of the samples were measured on the Micromeritics ASAP 2020 instrument. The morphology was observed on the Zeiss MERLIN compact field emission scanning electron microscope (FE-SEM) and a JEOL JEM 2100 plus transmission electron microscope (TEM). The X-ray diffraction (XRD) was performed on the Rigaku Ultima IV instrument, with a tube voltage of 40 kV, a tube current of 40 mA, and Cu Kα radiation. X-ray photoelectron spectroscopy (XPS) was performed on the Thermo ESCALAB 250XI electronic energy spectrometer, with C1s binding energy (284.8 eV) for energy calibration, X-ray source voltage of 16 kV, current of 14.9 mA, beam diameter of 650 μm. The temperature programmed chemical adsorption/reduction (TPD/TPR) was performed on the AutoChem1 II 2920 instrument. For NH<sub>3</sub>-TPD, the catalyst was pre-treated under argon atmosphere at 350 °C for 1 h, then cooled down to 50 °C and adsorbed NH<sub>3</sub> to saturation. After that the temperature was raised to 100 °C and the catalyst was purged with Ar gas to desorb the physically adsorbed NH<sub>3</sub>. Finally the temperature was raised to 500 °C at a ramping rate of 10 °C min<sup>−1</sup> and the outlet NH<sub>3</sub> concentration was detected by the thermal conductivity detector (TCD). For H<sub>2</sub>-TPR, the catalyst was pre-treated under Ar atmosphere at 350 °C for 1 h to remove the adsorbed gas on the surface, then cooled to room temperature. Then the catalyst was reduced in 10% H<sub>2</sub>/Ar atmosphere from room temperature to 800 °C at a ramping rate of 10 °C min<sup>−1</sup>. The H<sub>2</sub> consumption was detected by TCD.

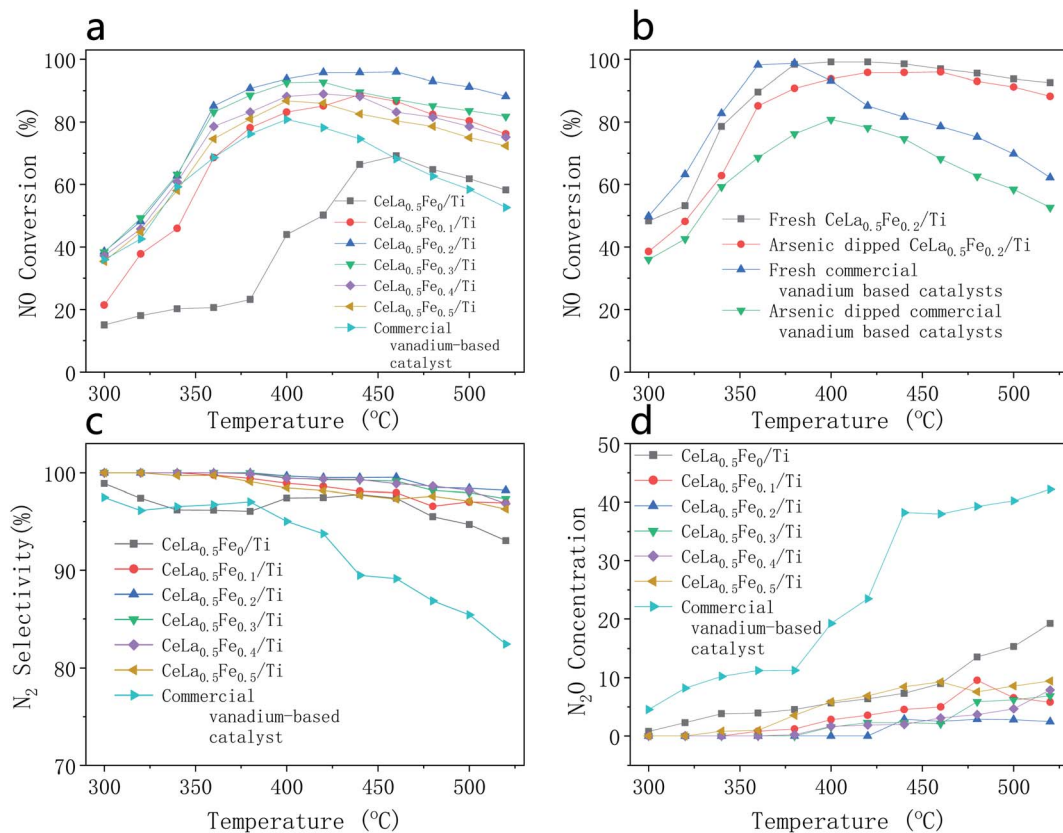


**Fig. 1** Catalytic performance of catalysts with different components, all the catalysts were treated by arsenic as described in Section 2.2 except "Fresh" catalysts. (a) NO conversion of  $\text{CeLa}_{0.5}\text{Fe}_x/\text{Ti}$  ( $x = 0, 0.1, 0.2, 0.3, 0.4, 0.5$ ) and commercial vanadium-based catalysts; (b) NO conversion of  $\text{CeLa}_{0.5}\text{Fe}_{0.2}/\text{Ti}$  and commercial vanadium-based catalyst with and without arsenic solution dipping; (c)  $\text{N}_2$  selectivity of  $\text{CeLa}_{0.5}\text{Fe}_x/\text{Ti}$  ( $x = 0, 0.1, 0.2, 0.3, 0.4, 0.5$ ) and commercial vanadium-based catalyst; (d)  $\text{N}_2\text{O}$  concentration of  $\text{CeLa}_{0.5}\text{Fe}_x/\text{Ti}$  ( $x = 0, 0.1, 0.2, 0.3, 0.4, 0.5$ ) and commercial vanadium-based catalyst.

### 3. Results and discussion

#### 3.1 Catalytic performance

Fig. 1 shows the catalytic performance of catalysts with different components, in which all the catalysts were treated by arsenic as described in Section 2.2 except "Fresh" catalysts. It can be seen from Fig. 1(a) that the loading of  $\text{Fe}_2\text{O}_3$  greatly improves the NO conversion. As temperature increases, the NO conversion first increases and then decreases. Influenced by the kinetics reason, the NO conversion will increase whereas the increasing trend will decrease with the increase of the temperature. If the temperature is too high ( $>450^\circ\text{C}$  for  $\text{CeLa}_{0.5}\text{Fe}_{0.2}/\text{Ti}$ ), the NO conversion will decrease due to the decrease of the  $\text{N}_2$  selectivity. At the same temperature, the NO conversion first increases and then decreases with the increase of the Fe content. When the  $\text{Fe}_2\text{O}_3$  content  $x$  is 0.2, the NO conversion of  $\text{CeLa}_{0.5}\text{Fe}_x/\text{Ti}$  is the highest. The temperature range where the corresponding NO conversion is greater than 80% of  $\text{CeLa}_{0.5}\text{Fe}_{0.2}/\text{Ti}$  is  $345\text{--}520^\circ\text{C}$ . Commercial vanadium-based catalyst shows much weaker arsenic resistance than  $\text{CeLa}_{0.5}\text{Fe}_{0.2}/\text{Ti}$ . On the one hand, Fe-based catalysts have good  $\text{deNO}_x$  performance,<sup>4,5</sup> on the other hand, Fe might form the bond of  $\text{Fe-O-As}^{6-9}$  with As, which makes Fe preferentially combine with As to protect the main active site of  $\text{CeO}_2$ . However, excessive loading of  $\text{Fe}_2\text{O}_3$  is detrimental to the  $\text{deNO}_x$  performance of the catalyst, which can be

attributed to the fact that excessive  $\text{Fe}_2\text{O}_3$  will cover the active sites of the  $\text{CeO}_2$  on the catalyst surface. Above  $350^\circ\text{C}$ , the NO conversion of the catalyst is maintained at a high level, which may be related to the enhanced oxidation of  $\text{CeO}_2$ .<sup>29</sup> The introduction of La increases the surface unsaturated oxygen on the surface and the dispersibility of  $\text{CeO}_2$ .<sup>30,31</sup> From Fig. 1(b), it can be found that the commercial vanadium-based catalyst is significantly poisoned in arsenic environment, while  $\text{CeLa}_{0.5}\text{Fe}_{0.2}/\text{Ti}$  catalyst is slightly affected in arsenic environment. The NO conversion of the  $\text{CeLa}_{0.5}\text{Fe}_{0.2}/\text{Ti}$  is obviously better than commercial vanadium-based catalyst with regard to the arsenic resistance. In Fig. 1(c), the  $\text{N}_2$  selectivity of the  $\text{CeLa}_{0.5}\text{Fe}_x/\text{Ti}$  ( $x = 0, 0.1, 0.2, 0.3, 0.4, 0.5$ ) catalysts is much better than that of commercial vanadium-based catalyst and  $\text{CeLa}_{0.5}\text{Fe}_{0.2}/\text{Ti}$  shows the best  $\text{N}_2$  selectivity (99.08–100%). In Fig. 1(d), the  $\text{N}_2\text{O}$  concentration of vanadium-based catalysts increases quickly whereas the  $\text{N}_2\text{O}$  concentrations of  $\text{CeLa}_{0.5}\text{Fe}_x/\text{Ti}$  ( $x = 0, 0.1, 0.2, 0.3, 0.4, 0.5$ ) increase slowly. This arsenic poisoning of vanadium-based catalysts is consistent with the results reported in the literature.<sup>4</sup>

#### 3.2 XRD

Fig. 2 shows the XRD pattern of  $\text{CeLa}_{0.5}\text{Fe}_x/\text{Ti}$  ( $x = 0, 0.1, 0.2$ ) series. The main phase of the three catalysts is anatase  $\text{TiO}_2$  (JCPDS no. 99-0008). The broad diffraction peaks indicate that

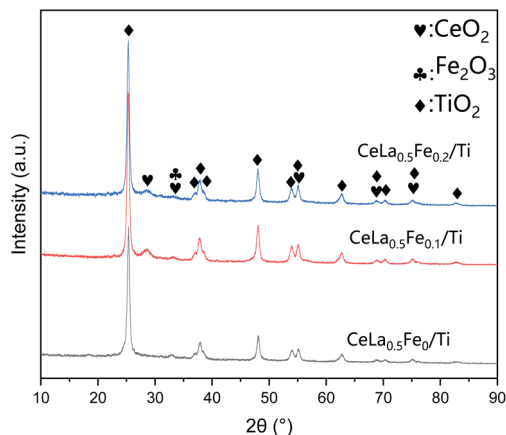


Fig. 2 XRD pattern of  $\text{CeLa}_{0.5}\text{Fe}_x/\text{Ti}$  ( $x = 0, 0.1, 0.2$ ) series.

the anatase is a nano-particle, which is consistent with the following SEM and TEM results. There are weaker cubic fluorite  $\text{CeO}_2$  peaks (JCPDS no. 43-1002) near  $28.6^\circ$ ,  $33^\circ$ , etc. The full width at half maximum (FWHM) of  $\text{CeO}_2$  is wider than that of anatase, showing that the grain size of  $\text{CeO}_2$  is much smaller than that of  $\text{TiO}_2$ . However, there is no phase related to the

$\text{La}_2\text{O}_3$ , indicating that  $\text{La}_2\text{O}_3$  is highly dispersed on the catalyst surface in an amorphous state, which is similar to the literature.<sup>32</sup> The XRD peak of  $\text{Fe}_2\text{O}_3$  ( $\sim 33.15^\circ$ , JCPDS no. 33-0664) is very weak and very wide, which indicates the  $\text{Fe}_2\text{O}_3$  is amorphous. The FWHM of the (111) peak of the  $\text{CeO}_2$  at  $28.5^\circ$  becomes wider with the increase of the Fe content, which means the addition of Fe decreases the  $\text{CeO}_2$  grain size. Since  $\text{CeO}_2$  is the main catalyst, small crystal size is beneficial to increase its catalytic activity. In addition, the peak of  $\text{CeO}_2$  at  $28.5^\circ$  (after Gaussian fitting) moves towards higher angle direction, which might be caused by the formation of the solid solution of  $\text{CeO}_2\text{-Fe}_2\text{O}_3$ . This is because the radius of  $\text{Ce}^{4+}$  (eight-coordinated,  $0.97 \text{ \AA}$ ) is larger than that of  $\text{Fe}^{3+}$  (eight-coordinated,  $0.78 \text{ \AA}$ ). It is worth noting that although there are reports in the literature that anatase will transform into rutile at  $\sim 500^\circ\text{C}$ ,<sup>33</sup> the rutile phase cannot be found in the catalysts, showing that the catalysts have good thermal stability.

### 3.3 SEM

Fig. 3 is the SEM images of the  $\text{CeLa}_{0.5}\text{Fe}_x/\text{Ti}$  ( $x = 0, 0.1, 0.2$ ) series. According to the reports, the catalysts with the size of nano-particles can show high catalytic activity.<sup>34</sup> As can be seen, the active components are highly dispersed on the surface of the

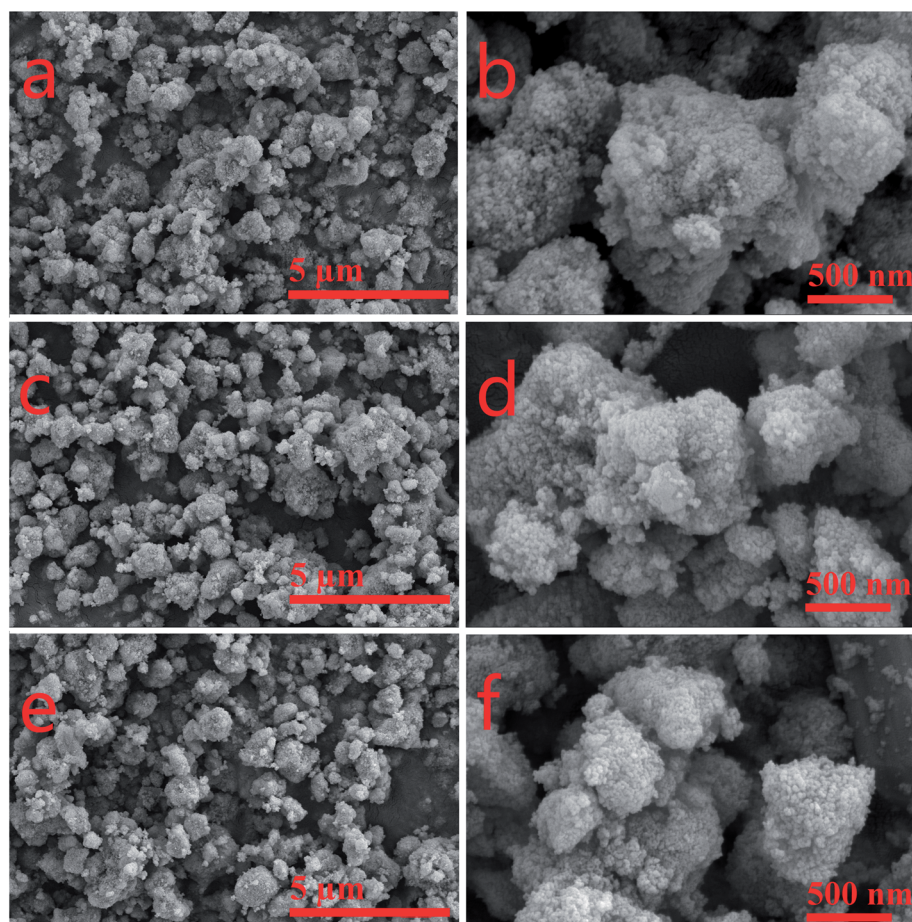


Fig. 3 SEM images of  $\text{CeLa}_{0.5}\text{Fe}_x/\text{Ti}$  ( $x = 0, 0.1, 0.2$ ) with different magnification. (a and b)  $\text{CeLa}_{0.5}\text{Fe}_0/\text{Ti}$ ; (c and d)  $\text{CeLa}_{0.5}\text{Fe}_{0.1}/\text{Ti}$ ; (e and f)  $\text{CeLa}_{0.5}\text{Fe}_{0.2}/\text{Ti}$ .

catalysts and the nano-particles form agglomerates with the size of sub-microns. The number of particles increases with the increase of the Fe content, which means that the addition of Fe may enhance the dispersion of CeO<sub>2</sub> on the surface of TiO<sub>2</sub>. This is consistent with the XRD results.

### 3.4 TEM

Fig. 4 shows the TEM image, elemental mapping, and energy dispersive spectra (EDS) of CeLa<sub>0.5</sub>Fe<sub>0.2</sub>/Ti. The morphology in Fig. 4(a) clearly shows that the crystal size of the catalyst is tens of nanometers. In the HR-TEM image (Fig. 4(b)), the stripe spacing of 0.357 nm corresponds to the (101) plane of anatase TiO<sub>2</sub>, and the stripe spacing about 0.318 nm corresponds to the (111) plane of CeO<sub>2</sub>. The elemental mapping pictures of Ti, Ce, Fe, La, and O (Fig. 4(d-h)) show that the La, Ce, Fe and Ti elements are uniformly distributed in the catalysts. The EDS result in Fig. 4(i) shows that the main elements are Ti, La, Ce, Fe, and Cu, where Cu is caused by the Cu grid used to support the sample.

### 3.5 XPS

Fig. 5 is the XPS spectra of CeLa<sub>0.5</sub>Fe<sub>x</sub>/Ti ( $x = 0, 0.1, 0.2$ ). The peaks of Ce, La, Ti, Fe and C can be found in the survey spectra

in Fig. 5(a). The Ce3d XPS spectra (Fig. 5(b)) can be fitted to nine peaks, named V<sub>1</sub> ( $\approx 880.7$  eV), V<sub>2</sub> ( $\approx 882.3$  eV), V<sub>3</sub> ( $\approx 885.8$  eV), V<sub>4</sub> ( $\approx 888.6$  eV), V<sub>5</sub> ( $\approx 898.3$  eV), U<sub>1</sub> ( $\approx 900.8$  eV), U<sub>2</sub> ( $\approx 903$  eV), U<sub>3</sub> ( $\approx 907.3$  eV), U<sub>4</sub> ( $\approx 916.7$  eV). All V peaks correspond to Ce3d<sub>5/2</sub> spin orbits, and all U peaks correspond to Ce3d<sub>3/2</sub> spin orbits. The peaks of V<sub>1</sub>, V<sub>3</sub>, and U<sub>2</sub> correspond to Ce<sup>3+</sup>, while the peaks of V<sub>2</sub>, V<sub>4</sub>, V<sub>5</sub>, U<sub>1</sub>, U<sub>3</sub>, and U<sub>4</sub> correspond to Ce<sup>4+</sup>.<sup>35</sup> From the peak area, the Ce<sup>3+</sup> content on the CeO<sub>2</sub> surface increases significantly as the Fe content increases. Because of the different electrovalence of Fe<sup>3+</sup> and Ce<sup>4+</sup>, in order to maintain charge balance, the oxygen vacancy defects on the CeO<sub>2</sub> surface also increase as the Fe content increases, which are beneficial to the improvement of the catalytic activity.<sup>36</sup> The XPS of O1s (Fig. 5(c)) can be fitted into two peaks: O<sub>α</sub> (surface unsaturated oxygen,  $\approx 530.6$  eV) and O<sub>β</sub> (lattice oxygen,  $\approx 528.7$  eV). Calculated by the fitted peak area, the O<sub>α</sub>/(O<sub>α</sub> + O<sub>β</sub>) fractions of CeLa<sub>0.5</sub>Fe<sub>0</sub>Ti, CeLa<sub>0.5</sub>Fe<sub>0.1</sub>Ti, CeLa<sub>0.5</sub>Fe<sub>0.2</sub>/Ti catalysts are 43.30%, 43.73% and 43.78%, respectively. Because the surface unsaturated oxygen O<sub>α</sub> of CeO<sub>2</sub> has a higher mobility and a stronger catalytic performance than the lattice oxygen O<sub>β</sub>, CeLa<sub>0.5</sub>Fe<sub>0.2</sub>/Ti catalyst shows the best catalytic performance.<sup>37</sup> In Fig. 5(d), the peaks of Fe2p correspond to Fe2p<sub>1/2</sub> (724 eV),

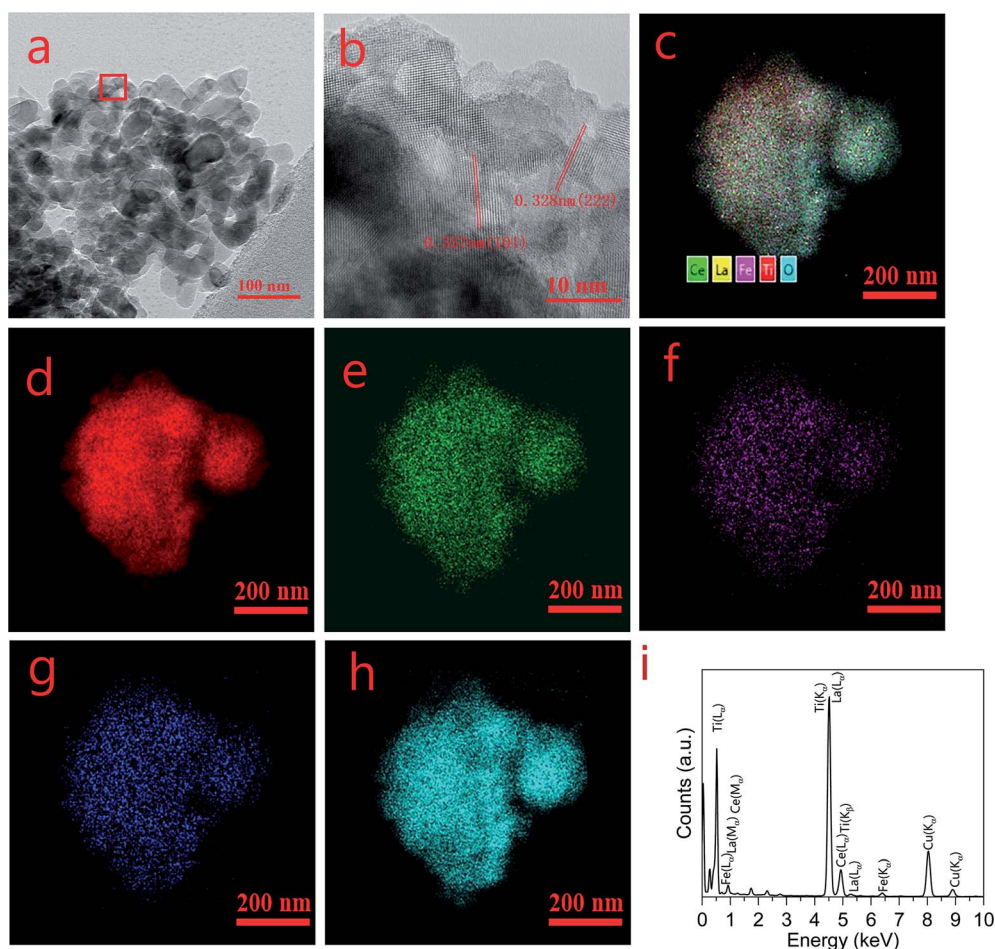


Fig. 4 TEM images, elemental mapping, and EDS of CeLa<sub>0.5</sub>Fe<sub>0.2</sub>/Ti. (a) TEM morphology, (b) HR-TEM, (c) all elements mapping, (d) Ti mapping, (e) Ce mapping, (f) Fe mapping, (g) La mapping, (h) O mapping. (i) EDS.

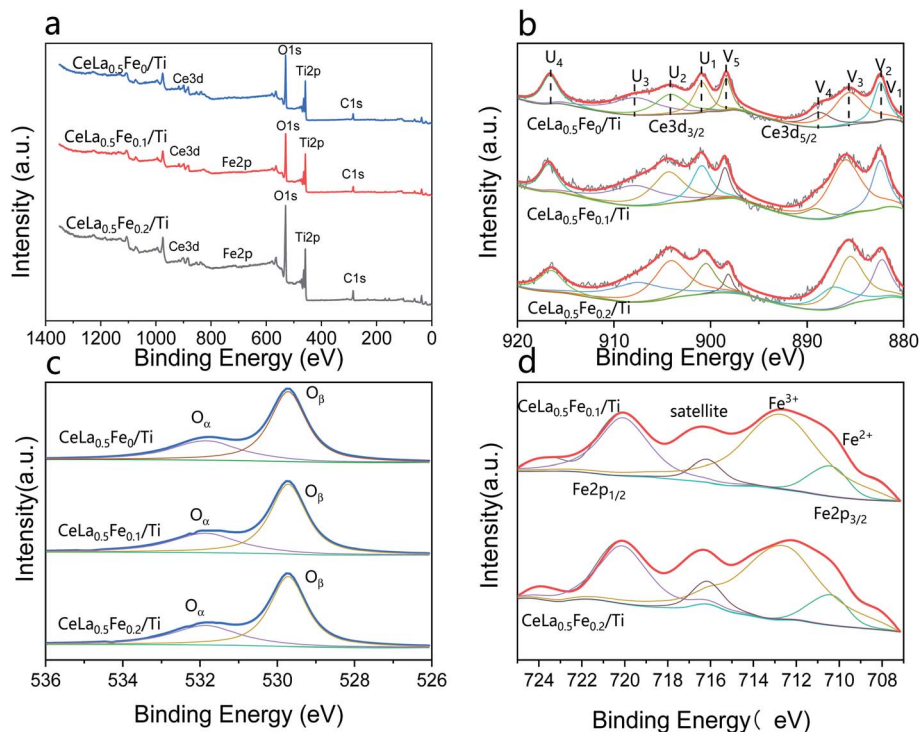


Fig. 5 XPS spectra of CeLa<sub>0.5</sub>Fe<sub>x</sub>/Ti ( $x = 0, 0.1, 0.2$ ). (a) Survey spectra; (b) Ce3d; (c) O1s; (d) Fe2p.

Fe2p<sub>3/2</sub> (711 eV) and satellite peaks. The peaks of Fe2p<sub>3/2</sub> are fitted by two peaks of Fe<sup>2+</sup> (710.0 eV) and Fe<sup>3+</sup> (712.8 eV).<sup>38</sup> The CeLa<sub>0.5</sub>Fe<sub>0.2</sub>/Ti and CeLa<sub>0.5</sub>Fe<sub>0.1</sub>/Ti catalysts have no obvious differences in shape and positions, showing that the valences of Fe in the two samples are the same or similar. No obvious satellite peak and asymmetric peak are observed at ~715 eV, and the peak positions of 2p<sub>3/2</sub>, satellite, and 2p<sub>1/2</sub> are close to that of Fe<sup>3+</sup>. However the existence of Fe<sup>2+</sup> must be considered because Fe<sup>2+</sup> can be fitted in the curve. Therefore, it can be concluded that Fe<sup>3+</sup> is the major valence while Fe<sup>2+</sup> is the minor valence on the surface.<sup>39</sup>

### 3.6 N<sub>2</sub> adsorption and desorption

The BET specific surface area, pore volume and pore diameter of CeLa<sub>0.5</sub>Fe<sub>x</sub>/Ti ( $x = 0, 0.1, 0.2$ ) series were measured by N<sub>2</sub> adsorption and desorption experiments. The results were shown in Table 1. Because the main components of the catalysts are TiO<sub>2</sub>, CeO<sub>2</sub> and La<sub>2</sub>O<sub>3</sub>, and the content of Fe<sub>2</sub>O<sub>3</sub> is very little, the change of Fe content has little effect on the specific surface area of the catalyst. The specific surface area increases and the pore size increases slightly. The reason may be that the

Table 1 BET specific surface area, pore volume and pore diameter of CeLa<sub>0.5</sub>Fe<sub>x</sub>/Ti ( $x = 0, 0.1, 0.2$ ) series

Catalyst	$S_{\text{BET}}$ (m <sup>2</sup> g <sup>-1</sup> )	$V_p$ (cm <sup>3</sup> g <sup>-1</sup> )	$D_p$ (nm)
CeLa <sub>0.5</sub> Fe <sub>0</sub> /Ti	78.1	0.040	3.25
CeLa <sub>0.5</sub> Fe <sub>0.1</sub> /Ti	79.7	0.039	3.28
CeLa <sub>0.5</sub> Fe <sub>0.2</sub> /Ti	79.9	0.041	3.32

introduction of Fe inhibits the growth rate of ceria grains and reduces the ceria grain size. This is consistent with the results of the XRD and SEM images.

### 3.7 NH<sub>3</sub>-TPD and H<sub>2</sub>-TPR

NH<sub>3</sub>-TPD result reflects the acidity of the catalysts. Fig. 6(a) shows the NH<sub>3</sub>-TPD curves of the CeLa<sub>0.5</sub>Fe<sub>x</sub>/Ti ( $x = 0, 0.1, 0.2, 0.3$ ) catalysts. As can be seen, the CeLa<sub>0.5</sub>Fe<sub>0</sub>/Ti catalyst has two desorption peaks at about 350 °C and 290 °C. It is generally believed that the peak above 450 °C is related to the Lewis acid site (strong acid site) associated with the NH<sub>3</sub> molecule, and the peak near 300 °C is related to the Brønsted acid site (weak acid site) associated with NH<sub>4</sub><sup>+</sup> ions.<sup>40</sup> From the peak area, the quantity of the Brønsted acid sites on the surface of the catalyst increases with the increase of Fe content up to  $x = 0.2$ , which helps to increase the catalytic activity. This is consistent with the catalytic performance in Fig. 1.

H<sub>2</sub>-TPR result reflects the redox characteristics of the catalysts. Fig. 6(b) shows the H<sub>2</sub>-TPR curves of the CeLa<sub>0.5</sub>Fe<sub>x</sub>/Ti ( $x = 0, 0.1, 0.2, 0.3$ ) catalysts. The strong peaks of the four catalysts in the range of 450–580 °C correspond to the reduction process from Ce<sup>4+</sup> to Ce<sup>3+</sup>, which are closely related to the catalytic activity of the catalysts.<sup>41</sup> With the increase of Fe content  $x$  up to  $x = 0.2$ , the peak position shifts towards lower temperature direction from 577 °C to 473 °C, which means that the introduction of Fe makes the reduction of the surface oxygen on CeO<sub>2</sub> by H<sub>2</sub> more easy. However, when the Fe content increases to  $x = 0.3$ , the reduction peak changes from 473 °C to 515 °C, which means that the reduction of CeO<sub>2</sub> on the catalyst surface becomes more difficult. From the peak area, the H<sub>2</sub>

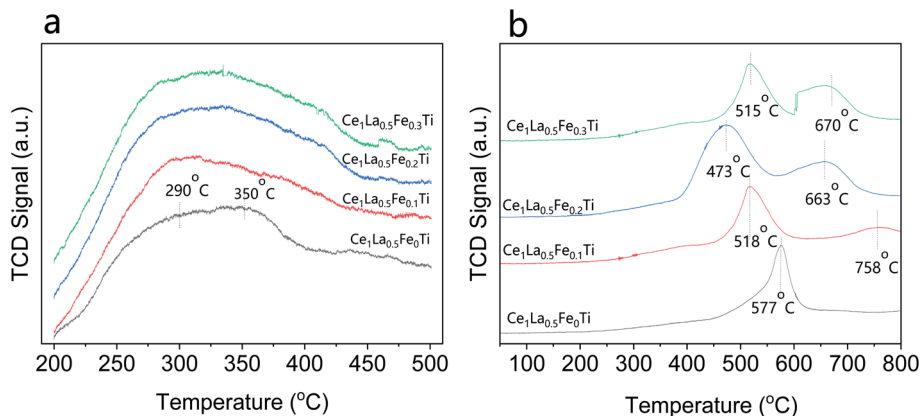


Fig. 6 (a)  $\text{NH}_3$ -TPD curves of the  $\text{CeLa}_{0.5}\text{Fe}_x/\text{Ti}$  ( $x = 0, 0.1, 0.2, 0.3$ ) catalysts; (b)  $\text{H}_2$ -TPR curves of the  $\text{CeLa}_{0.5}\text{Fe}_x/\text{Ti}$  ( $x = 0, 0.1, 0.2, 0.3$ ) catalysts.

consumption is  $\text{CeLa}_{0.5}\text{Fe}_{0.2}/\text{Ti} > \text{CeLa}_{0.5}\text{Fe}_{0.3}/\text{Ti} > \text{CeLa}_{0.5}\text{Fe}_{0.1}/\text{Ti} > \text{CeLa}_{0.5}\text{Fe}_0/\text{Ti}$ , showing that the surface oxygen on  $\text{CeO}_2$  increases with the increase of Fe content, which is consistent with the XPS results. Based on the  $\text{NH}_3$ -TPD and  $\text{H}_2$ -TPR curves, it can be concluded that  $\text{CeLa}_{0.5}\text{Fe}_{0.2}/\text{Ti}$  catalyst has the most acidic sites and strongest redox performance.

## 4. Conclusions

An anti-arsenic SCR denitration catalyst with anatase as the carrier,  $\text{CeO}_2$ , as the main active components, and  $\text{La}_2\text{O}_3$ ,  $\text{Fe}_2\text{O}_3$  as the main auxiliary agent was prepared by the impregnation method. The optimized  $\text{CeLa}_{0.5}\text{Fe}_{0.2}/\text{Ti}$  catalyst exhibits better catalytic performance under arsenic environment than the commercial vanadium-based catalysts. After the introduction of the  $\text{Fe}_2\text{O}_3$ , the  $\text{Ce}^{3+}$  concentration, surface unsaturated oxygen,  $\text{CeO}_2$  dispersibility, specific surface area, and acidic sites are all improved, which improves the catalytic activity in the arsenic environment.  $\text{CeLa}_{0.5}\text{Fe}_{0.2}/\text{Ti}$  catalyst has high NO conversion efficiency, excellent  $\text{N}_2$  selectivity and arsenic resistance, which might be a candidate for SCR denitrification applications in the arsenic flue gas environment.

## Conflicts of interest

There are no conflicts to declare.

## Acknowledgements

The research was supported by the National Natural Science Foundation of China under grant no. 51708447, Key R&D Project of Shaanxi Province under grant no. 2019SF-250, and Major Scientific and Technological Innovation Projects of Shandong Province under grant no. 2019JZZY010343.

## References

1 S. Luo, W. Zhou, A. Xie, F. Wu and T. Liu, Effect of  $\text{MnO}_2$  polymorphs structure on the selective catalytic reduction of

$\text{NO}_x$  with  $\text{NH}_3$  over  $\text{TiO}_2$ -palygorskite, *Chem. Eng. J.*, 2016, **286**, 291–299.

- Z. Liu, J. Zhu, S. Zhang, L. Ma and S. I. Woo, Selective catalytic reduction of  $\text{NO}_x$  by  $\text{NH}_3$  over  $\text{MoO}_3$ -promoted  $\text{CeO}_2/\text{TiO}_2$  catalyst, *Catal. Commun.*, 2014, **46**, 90–93.
- G. Busca, L. Lietti, G. Ramis and F. Berti, Chemical and mechanistic aspects of the selective catalytic reduction of  $\text{NO}_x$  by ammonia over oxide catalysts: A review, *Appl. Catal., B*, 1998, **18**, 1–36.
- S. Brandenberger, O. Kröcher, A. Tissler and R. Althoff, The state of the art in selective catalytic reduction of  $\text{NO}_x$  by ammonia using metal-exchanged zeolite catalysts, *Catal. Rev.*, 2008, **50**, 492–531.
- P. Li, Y. Xin, Q. Li, Z. Wang, Z. Zhang and L. Zheng, Ce–Ti amorphous oxides for selective catalytic reduction of NO with  $\text{NH}_3$ : Confirmation of Ce–O–Ti active sites, *Environ. Sci. Technol.*, 2012, **46**, 9600–9605.
- R. Qu, X. Gao, K. Cen and J. Li, Relationship between structure and performance of a novel cerium-niobium binary oxide catalyst for selective catalytic reduction of NO with  $\text{NH}_3$ , *Appl. Catal., B*, 2013, **142**, 290–297.
- H. Li, C. Y. Wu, Y. Li and J. Zhang, Superior activity of  $\text{MnO}_x/\text{CeO}_2/\text{TiO}_2$  catalyst for catalytic oxidation of elemental mercury at low flue gas temperatures, *Appl. Catal., B*, 2012, **111**, 381–388.
- C. L. Senior, D. O. Lignell, A. F. Sarofim and A. Mehta, Modeling arsenic partitioning in coal-fired power plants, *Combust. Flame*, 2006, **147**, 209–221.
- E. Hums, Is advanced SCR technology at a standstill? A provocation for the academic community and catalyst manufacturers, *Catal. Today*, 1998, **42**, 25–35.
- Q. Lu, X. Q. Pei, Y. W. Wu, M. X. Xu, D. J. Liu and L. Zhao, Deactivation mechanism of the commercial  $\text{V}_2\text{O}_5\text{-MoO}_3/\text{TiO}_2$  selective catalytic reduction catalyst by arsenic poisoning in coal-fired power plants, *Energy Fuels*, 2020, **34**, 4865–4873.
- M. Kong, Q. C. Liu, X. Q. Wang, S. Ren, J. Yang, D. Zhao, W. C. Xi and L. Yao, Performance impact and poisoning mechanism of arsenic over commercial  $\text{V}_2\text{O}_5\text{-WO}_3/\text{TiO}_2$  SCR catalyst, *Catal. Commun.*, 2015, **72**, 121–126.

- 12 F. Hilbrig, H. E. Göbel, H. Knözinger, H. Schmelz and B. Lengeler, Interaction of arsenious oxide with DeNOx-catalysts: An X-ray absorption and diffuse reflectance infrared spectroscopy study, *J. Catal.*, 1991, **129**, 168–176.
- 13 S. Pritchard, S. Kaneko and K. Suyama, *Optimizing SCR catalyst design and performance for coal-fired boilers*, EPA/EPRI 1995 Joint Symposium Stationary Combustion NOx Control, May 16–19, 1995.
- 14 I. Morita, M. Hirano and B. H. K. K. Kure, *Development and commercial operating experience of SCR DeNOx catalysts for wet bottom coal fired boilers*, Power-Gen International, Dec 9–11, 1998.
- 15 E. Hums, A catalytically highly-active, arsenic oxide resistant V-Mo-O phase — results of studying intermediates of the deactivation process of V<sub>2</sub>O<sub>5</sub>-MoO<sub>3</sub>-TiO<sub>2</sub> (anatase) DeNO<sub>x</sub> catalysts, *Res. Chem. Intermed.*, 1993, **19**, 419–441.
- 16 Y. Peng, W. Si, X. Li, J. Luo, J. Li, J. Crittenden and J. Hao, Comparison of MoO<sub>3</sub> and WO<sub>3</sub> on arsenic poisoning V<sub>2</sub>O<sub>5</sub>/TiO<sub>2</sub> catalyst: DRIFTS and DFT study, *Appl. Catal., B*, 2016, **181**, 692–698.
- 17 Y. Peng, J. Li, W. Si, J. Luo, Q. Dai, X. Luo, X. Liu and J. Hao, Insight into deactivation of commercial SCR catalyst by arsenic: An experiment and DFT study, *Environ. Sci. Technol.*, 2014, **48**, 13895–13900.
- 18 X. Li, J. Li, Y. Peng, X. Li, K. Li and J. Hao, Comparison of the structures and mechanism of arsenic deactivation of CeO<sub>2</sub>-MoO<sub>3</sub> and CeO<sub>2</sub>-WO<sub>3</sub> SCR Catalysts, *J. Phys. Chem. C*, 2016, **120**, 18005–18014.
- 19 X. Li, J. Li, Y. Peng, H. Chang, T. Zhang, S. Zhao, W. Si and J. Hao, Mechanism of arsenic poisoning on SCR catalyst of CeW/Ti and its novel efficient regeneration method with hydrogen, *Appl. Catal., B*, 2016, **184**, 246–257.
- 20 X. Li, X. Li, J. Li and J. Hao, Identification of the arsenic resistance on MoO<sub>3</sub> doped CeO<sub>2</sub>/TiO<sub>2</sub> catalyst for selective catalytic reduction of NO<sub>x</sub> with ammonia, *J. Hazard. Mater.*, 2016, **318**, 615–622.
- 21 G. H. Yao, K. T. Gui and F. Wang, Low-temperature de-NO<sub>x</sub> by selective catalytic reduction based on iron-based catalysts, *Chem. Eng. Technol.*, 2010, **33**, 1093–1098.
- 22 M. Devadas, O. Kröcher, M. Elsener, A. Wokaun, G. Mitrikas, N. Söger, M. Pfeifer, Y. Demel and L. Mussmann, Characterization and catalytic investigation of Fe-ZSM5 for urea-SCR, *Catal. Today*, 2007, **119**, 137–144.
- 23 Z. C. Li, X. M. Liu, W. Jin, Q. S. Hu and Y. P. Zhao, Adsorption behavior of arsenicals on MIL-101(Fe): The role of arsenic chemical structures, *J. Colloid Interface Sci.*, 2019, **554**, 692–704.
- 24 M. A. V. Ramos, W. Yan, X. Li and B. Koel, Simultaneous oxidation and reduction of arsenic by zero-valent iron nanoparticles: understanding the significance of the core-shell structure, *J. Phys. Chem. C*, 2009, **113**, 14591–14594.
- 25 H. P. Feng, L. Tang, J. Tang, G. M. Zeng, H. Dong, Y. C. Deng, L. L. Wang, Y. N. Liu, X. Y. Ren and Y. Y. Zhou, Cu-doped Fe@Fe<sub>2</sub>O<sub>3</sub> core-shell nanoparticle shifted oxygen reduction pathway for high-efficiency arsenic removal in smelting wastewater, *Environ. Sci.: Nano*, 2018, **5**, 1595–1607.
- 26 M. J. Uddin and Y. K. Jeong, Review: Efficiently performing periodic elements with modern adsorption technologies for arsenic removal, *Environ. Sci. Pollut. Res.*, 2020, **27**, 39888–39912.
- 27 Z. Liu, S. Zhang, J. Li and L. Ma, Promoting effect of MoO<sub>3</sub> on the NO<sub>x</sub> reduction by NH<sub>3</sub> over CeO<sub>2</sub>/TiO<sub>2</sub> catalyst studied with in situ DRIFTS, *Appl. Catal., B*, 2014, **144**, 90–95.
- 28 W. Shan, F. Liu, H. He, X. Shi and C. Zhang, A superior Ce-W-Ti mixed oxide catalyst for the selective catalytic reduction of NO<sub>x</sub> with NH<sub>3</sub>, *Appl. Catal., B*, 2012, **115–116**, 100–106.
- 29 J. W. Shi, Y. Wang, R. B. Duan, C. Gao, B. R. Wang, C. He and C. M. Niu, The synergistic effects between Ce and Cu in Cu<sub>y</sub>Ce<sub>1-y</sub>W<sub>5</sub>O<sub>x</sub> catalysts for enhanced NH<sub>3</sub>-SCR of NO<sub>x</sub> and SO<sub>2</sub> tolerance, *Catal. Sci. Technol.*, 2019, **9**, 718–730.
- 30 B. Zhang, D. Li and X. Wang, Catalytic performance of La-Ce-O mixed oxide for combustion of methane, *Catal. Today*, 2010, **158**, 348–353.
- 31 Y. Dai, X. Y. Wang, D. Li and Q. G. Dai, Catalytic combustion of chlorobenzene over Mn-Ce-La-O mixed oxide catalysts, *J. Hazard. Mater.*, 2011, **188**, 132–139.
- 32 L. Gao, C. Li, P. Lu, J. Zhang, X. Du, S. Li, L. Tang, J. Chen and G. Zeng, Simultaneous removal of Hg<sup>0</sup> and NO from simulated flue gas over columnar activated coke granules loaded with La<sub>2</sub>O<sub>3</sub>-CeO<sub>2</sub> at low temperature, *Fuel*, 2018, **215**, 30–39.
- 33 O. Carp, C. L. Huisman and A. Reller, Photoinduced reactivity of titanium dioxide, *Prog. Solid State Chem.*, 2004, **32**, 33–177.
- 34 Z. Yan, J. Wang, R. Zou, L. Liu, Z. Zhang and X. Wang, Hydrothermal synthesis of CeO<sub>2</sub> nanoparticles on activated carbon with enhanced desulfurization activity, *Energy Fuels*, 2012, **26**, 5879–5886.
- 35 A. Gupta, M. Hegde, K. Priolkar, U. Waghmare, P. Sarode and S. Emura, Structural investigation of activated lattice oxygen in Ce<sub>1-x</sub>Sn<sub>x</sub>O<sub>2</sub> and Ce<sub>1-x</sub>Sn<sub>x</sub>Pd<sub>y</sub>O<sub>2-δ</sub> by EXAFS and DFT calculation, *Chem. Mater.*, 2009, **21**, 5836–5847.
- 36 T. Montini, M. Melchionna, M. Monai and P. Fornasiero, Fundamentals and catalytic applications of CeO<sub>2</sub>-based materials, *Chem. Rev.*, 2016, **116**, 5987–6041.
- 37 F. Liu, H. He, Y. Ding and C. Zhang, Effect of manganese substitution on the structure and activity of iron titanate catalyst for the selective catalytic reduction of NO with NH<sub>3</sub>, *Appl. Catal., B*, 2009, **93**, 3760–3769.
- 38 Z. H. Chen, F. R. Wang, H. Li, Q. Yang and L. F. Wang, Low-temperature selective catalytic reduction of NO<sub>x</sub> with NH<sub>3</sub> over Fe-Mn mixed-oxide catalysts containing Fe<sub>3</sub>Mn<sub>3</sub>O<sub>8</sub> phase, *Ind. Eng. Chem. Res.*, 2012, **51**, 202–212.
- 39 M. T. Van Dongen, D. Ng, L. V. Moura, D. Acharya, J. Wang, C. D. Easton, F. Wang and Z. Xie, Synthesis and characterisation of monolithic PTFE-modified MnO<sub>x</sub>/FeO<sub>x</sub> catalysts for selective catalytic reduction (SCR) of NO<sub>x</sub> at low temperature, *J. Chem. Technol. Biotechnol.*, 2021, DOI: 10.1002/jctb.6612.
- 40 R. Zhang, W. Yang, N. Luo, P. Li, Z. Lei and B. Chen, Low-temperature NH<sub>3</sub>-SCR of NO by lanthanum manganite perovskites: Effect of A/B-site substitution and TiO<sub>2</sub>/CeO<sub>2</sub> support, *Appl. Catal., B*, 2014, **146**, 94–104.
- 41 Z. Liu, J. Zhu, J. Li, L. Ma and S. I. Woo, Novel Mn-Ce-Ti mixed-oxide catalyst for the selective catalytic reduction of NO<sub>x</sub> with NH<sub>3</sub>, *ACS Appl. Mater. Interfaces*, 2016, **283**, 1044–1050.